Atmos. Chem. Phys. Discuss., 14, 18083–18126, 2014
www.atmos-chem-phys-discuss.net/14/18083/2014/
doi:10.5194/acpd-14-18083-2014

Atmospheric Chemistry and Physics Discussions

Surface-to-mountaintop transport characterised by radon observations at the Jungfraujoch

A. D. Griffiths[1], F. Conen[2], E. Weingartner[3,*], L. Zimmermann[2], S. D. Chambers[1], and A. G. Williams[1]

[1]Australian Nuclear Science and Technology Organisation, New South Wales, Australia
[2]Environmental Geosciences, Department of Geosciences, University of Basel, Switzerland
[3]Laboratory of Atmospheric Chemistry, Paul Scherrer Institute, 5232 Villigen, Switzerland
[*]now at: Institute for Aerosol and Sensor Technology, University of Applied Sciences, 5210 Windisch, Switzerland

Received: 5 May 2014 – Accepted: 22 June 2014 – Published: 4 July 2014

Correspondence to: A. D. Griffiths (alan.griffiths@ansto.gov.au)

Published by Copernicus Publications on behalf of the European Geosciences Union.

Abstract

Atmospheric composition measurements at Jungfraujoch are affected intermittently by thermally-driven (anabatic) mountain winds as well as by other vertical transport mechanisms. Using radon-222 observations, and a new analysis method, we quantify the land surface influence hour-by-hour and detect the presence of anabatic winds on a daily basis. During 2010–2011, anabatic winds occurred on roughly 40 % of days, but only from April–September. Anabatic wind days were associated with warmer air temperatures over a large fraction of Europe and with a shift in airmass properties. Shifts were evident even when comparing the same radon concentrations, a proxy for land-surface influence. Aerosol washout, when quantified as a function of rain-rate using a radon normalisation technique, was also influenced by anabatic winds being more pronounced on non-anabatic days. Excluding the influence of anabatic winds, however, did not lead to a better definition of the unperturbed aerosol background than a definition based on radon alone, supporting the use of a radon threshold to identify periods with weak land-surface influence.

1 Introduction

High altitude mountain sites have long been recognised as good places for atmospheric composition measurements. Primarily influenced by distant sources, such sites can be used to make measurements which are representative of the global average concentration (Keeling et al., 1976), also known as the baseline (Calvert, 1990). But local sources can also be important, depending largely on the recent history of vertical transport and associated mixing.

The difficult task of understanding vertical transport is further complicated by mountains, or mountain ranges, which affect vertical exchange processes (Rotach and Zardi, 2007; Weissmann et al., 2005) in site-specific ways which are not as well understood as processes occurring over flat terrain (Zardi and Whiteman, 2013). As a consequence,

ACPD
14, 18083–18126, 2014

Stohl et al. (2009) found that mountain-top measurements were less use than measurements at flat sites, for constraining regional estimates of greenhouse gas emissions.

At the High Altitude Research Station Jungfraujoch, a key European and Global Atmospheric Watch monitoring site, local influences become important during periods of enhanced vertical transport and need to be reliably accounted for during data interpretation. The site is located in a saddle, 3454 m a.s.l., on the north-west flank of the Swiss Alps (Fig. 1). Below station elevation, winds over the Swiss Plateau are channelled parallel to the mountain range, whereas above mountain tops winds are most frequently from the north-west, with a broad unimodal maximum (Furger, 1992; Ketterer et al., 2014). At Jungfraujoch itself, however, the wind direction distribution is bimodal due to the site's position in the saddle.

Although air sampled at Jungfraujoch is largely representative of the free troposphere, there is a a seasonally-varying local influence that is strongest in summer (Collaud Coen et al., 2011; Lugauer et al., 1998).

The pollution observed at Jungfraujoch is contributed to from many sources. There are nearby aerosol sources on the Swiss Plateau and in the Rhône Valley (De Wekker et al., 2004), sources of various species to the south from the Po Valley (Reimann et al., 2008, 2004; Seibert et al., 1998) and regional-scale European sources, mainly in Switzerland, France and Germany (Uglietti et al., 2011). In addition to these surface sources, stratospheric incursions can affect air composition, especially ozone (Stohl et al., 2000; Trickl et al., 2010).

The three primary transport mechanisms (Forrer et al., 2000), most relevant to the chemical and meteorological processes observed at Jungfraujoch (Zellweger et al., 2003), are:

1. Thermally-driven boundary-layer growth and anabatic mountain winds (Henne et al., 2004, 2005; Collaud Coen et al., 2011; De Wekker et al., 2004; Weigel et al., 2006; Kossmann et al., 1999; Zellweger et al., 2000).

ACPD
14, 18083–18126, 2014

2. Dynamically-driven winds, including föhn winds, where synoptic winds interact with terrain (Drobinski et al., 2007; Campana et al., 2005; Lothon et al., 2003)

3. Vertical mixing over flat terrain followed by advection to the Alps; such as in the case of deep convection (active cumulus, or cumulonimbus formation), or associated with frontal systems (Purvis et al., 2003), of which the Iberian Peninsula is a major source region (Cui et al., 2011).

Thermal forcing, the focus of this study, is most common under clear sky, low wind conditions in summer, when incoming solar radiation is strong. As well as the development of a deep convective boundary layer over the surrounding flat terrain, heating of the mountain slopes leads to a net buoyancy force, driving anabatic upslope winds (Haiden, 2003; Mahrt, 1982). Anabatic winds transport air up valleys, enhancing vertical exchange by a factor of three compared with flat terrain (Weigel et al., 2006), and convergence near mountain peaks further enhances the export of boundary layer air to the free troposphere.

In aggregate, mountain ranges create an injection layer above and in their lee (Henne et al., 2005; Nyeki et al., 2000) which is dynamically decoupled from the convective boundary layer but has similar tracer concentrations. In order to feed the vertical transport, air from within ~ 80 km is drawn horizontally towards the base of the mountains over the course of a day (Weissmann et al., 2005); the export of mass to the troposphere is significant at a regional scale.

There has been an ongoing effort to characterise the local influences on Jungfraujoch observations. Previous workers have employed in situ measurements of surface-emitted tracers with a strong concentration contrast between the boundary layer and free troposphere, such as aerosols (Collaud Coen et al., 2011), CO (Prévôt et al., 2000), and moisture (Henne et al., 2004, 2005) while others have incorporated back-trajectories (Balzani Lööv et al., 2008; Kossmann et al., 1999; Cui et al., 2011). While back-trajectories have proven to be effective during the winter months they have been unable to resolve anabatic mountain winds. Consequently, meteorological or time-of-

ACPD
14, 18083–18126, 2014

day filters (Andrews et al., 2011; Zellweger et al., 2003) have been used to avoid periods influenced by anabatic winds. Yet another approach has been to relate synoptic weather classifications to the occurrence of vertical transport (Collaud Coen et al., 2011). Data augmenting in situ measurements has included lidar, used to detect the top of aerosol layers (Nyeki et al., 2000; Gallagher et al., 2012; Ketterer et al., 2014), and radiosondes, which are launched from near the mountain and used to define the unperturbed free troposphere (Weiss-Penzias et al., 2006).

In this study we employ radon–222 (radon hereafter), an inert radioactive gas emitted from the ice-free land surface, and examine how useful it is for detecting anabatic winds at Jungfraujoch. Lugauer et al. (2000) demonstrated the feasibility of this approach, at Jungfraujoch, by measuring radon decay products attached to aerosol particles; with our method we are able to determine the concentration of radon itself, removing uncertainties due to the fraction of decay products which attach to aerosols, deposit on the ground, or remain airborne.

Although other tracers, aerosols or surface-emitted chemical species, have been used in a similar way, we hypothesise that radon is a more reliable tracer of surface influence; it is emitted by all soils at a relatively constant rate (Szegvary et al., 2007; Zhang et al., 2011), and its only significant sink is radioactive decay. With a half-life of 3.8 d, its atmospheric background concentration is low and temporal variations caused by changes in atmospheric transport are more clearly detectable than for other tracers with longer atmospheric lifetimes. Furthermore, seasonal snow cover attenuates emissions (Yamazawa et al., 2005) and we assume that emissions are negligible in the area with permanent snow cover surrounding Jungfraujoch, even though there are reports of sites above the snowline which allow radon to escape through from the bedrock below (Pourchet et al., 2000).

Radon has previously been used to study vertical mixing based on temporal variations (Griffiths et al., 2013), or vertical profiles from aircraft (Guedalia et al., 1972; Lee and Cicerone, 1997; Williams et al., 2011) towers (Chambers et al., 2011; Grossi et al., 2012; Williams et al., 2013) or sites with different altitudes (Chevillard et al., 2002).

ACPD
14, 18083–18126, 2014

Radon has been incorporated into transport models as an axillary diagnostic of mixing (Vogel et al., 2013), or for testing transport or parameterisations (Feichter and Crutzen, 1990; Zhang et al., 2008). Other applications of ground-based detectors are reviewed by (Zahorowski et al., 2004).

In a refinement of earlier studies, we first use the Jungfraujoch radon measurements to rank days according to the strength of anabatic winds, then – on the days of significant anabatic influence – use radon measurements from a second detector, at Bern on the Swiss Plateau, to verify the Jungfraujoch radon source. We then examine the implications of anabatic winds, showing that their detection can be linked to meteorological observations (Sect. 3.2), and that anabatic winds influence airmass properties (Sect. 3.3). Despite their successful identification and characterisation, we show that taking the presence of anabatic winds into account does not improve upon the identification of unperturbed baseline airmasses at Jungfraujoch as previously determined by the application of a purely radon-based selection threshold (Sect. 3.4).

2 Data and methods

2.1 Radon observations at Jungfraujoch and Bern

Radon detectors have been operated continuously at Bern and Jungfraujoch since 2009. Here we use two full years of data from 2011 and 2012. The instruments are of the two-filter dual flow loop design, with a delay chamber of 400 L to remove thoron and a radon detection chamber of 750 L (Whittlestone and Zahorowski, 1998). This design eliminates an uncertainty inherent to progeny detectors (Xia et al., 2010) but means that the detectors are large and have a relatively slow response time.

The detectors respond to a step change in ambient concentration with a one-half rise time of 30 min. Radon concentration, as a result, lags measurements made using faster sensors. We corrected for this by adjusting the calibrated radon concentrations by a lag (one hour) which maximised the correlation between radon and other tracers.

ACPD
14, 18083–18126, 2014

Operation of the detectors followed the protocol described by Chambers et al. (2011). Calibration was performed automatically every month by injecting a known amount of radon from a calibration source with an absolute uncertainty of 4 % (Pylon Electronics). Instrument background was measured every three months. As well as being necessary for converting counts into radon concentration, the instrument background determines the lower limit of detection, defined as the concentration with a counting error of 30 %. For these instruments, the lower limit of detector was about 40 mBq m^{-3}. At Jungfraujoch, where observed radon concentrations are $\gtrsim$ 100 mBq m^{-3} for 99 % of the time, the counting error is immaterial.

Calibrated radon concentrations were converted from activity concentration at ambient conditions (Bq m^{-3}) to a quantity which is conserved during an air parcel's ascent: activity concentration at standard temperature and pressure, 1013 hPa, 0 °C, written Bq m^{-3} STP.

2.2 Other parameters

A range of meteorological and air chemistry parameters are measured continuously at Jungfraujoch and on the plateau at Payerne. Some of these are archived in the EBAS database (NILU, 2012) and the World Data Centre for Greenhouse Gases (WDCGG; WMO, 2012). The measurements employed in this study were NO_y (chemiluminescence), N_2O (gas chromatography), CO (non-dispersive infra-red absorption), and standard meteorological observations downloaded from the WDCGG. We also use nephelometer measurements of the aerosol light scattering coefficient at 450 nm, from EBAS.

2.3 Transport simulations (back-trajectories)

Backwards trajectory simulations were performed using Hysplit version 4 (Draxler and Hess, 1998) forced with meteorological data at one-degree resolution from the NCEP Global Data Assimilation System (GDAS) model. The forcing data are six-hourly on

ACPD
14, 18083–18126, 2014

23 pressure levels (6 between 1000–850 hPa) and were accessed via the Hysplit website (ARL, 2013). The trajectories are primarily used as an indicator of synoptic-scale flow direction, characterised by the back-bearing to Jungfraujoch after reaching a distance of 61 km from the receptor (the distance between Bern and Jungfraujoch). The particle release height matches the station elevation, 3.5 km ASL, but is 2.2 km above the GDAS topography. Folini et al. (2008) discuss the impact of the chosen receptor height, observing that a choice close to the station elevation, rather than near the model ground level, is better at reproducing horizontal advection. In Sect. 3.5 we analyse rainfall along back-trajectories, which is obtained from the forecast component of the GDAS. We regard this as a crude approximation because of the low resolution of the wind fields, the complex topography, and the neglect of turbulent dispersion in the trajectory computation, but sufficient for our purposes.

2.4 Anabatic wind detection

2.4.1 Method description

In common with previous investigators (Prévôt et al., 2000; Gallagher et al., 2011) the central feature of our method is the recognition that anabatic mountain winds are associated with a diurnal cycle in tracer concentrations near mountain tops, peaking in the afternoon. However, while previous investigators, such as Gallagher et al. (2011), fitted a sinusoid to daily measurements, our approach avoids imposing constraints on the shape of the diurnal cycle. Furthermore, unlike Prévôt et al. (2000), who used CO as a surface tracer, we do not normalise by the near-surface value because of the relative homogeneity of radon emissions compared with CO.

The steps in the procedure are:

1. Gaps in the tracer time series are filled via linear interpolation, provided they are ≤ 3 h.

ACPD
14, 18083–18126, 2014

2. The time series is split into 24 h segments beginning at 07:00 UTC, the time of minimum radon concentration in the Jungfraujoch diurnal composite.

3. Segments with data gaps remaining are discarded.

4. Each segment has its mean subtracted and is placed in a set called the *input set*.

5. For each segment in the input set, a diurnal composite is computed from all segments in the input set except for the current one.

6. The segment whose exclusion reduces the composite's mean-squared value the most has its original mean value restored (the value subtracted in step 4) and is then transferred from the input set to an ordered *output list*, the first segment (or day) is given an anabatic rank of 1 and so on.

7. Steps 5 and 6 are repeated until the input set is empty.

In addition to ordering days by the importance of anabatic influence, as a secondary diagnostic the daily radon load is partitioned into three components. First a running diurnal composite is computed, intended to extract the influence of anabatic winds in the presence of unrelated fluctuations in radon concentration. The running diurnal composite for the day with anabatic rank i is computed from days ranked $i - 5$ to $i + 5$. The partitioning of radon concentration is illustrated in Fig. 2 with the components defined by:

1. Background radon, the minimum of the running diurnal composite.

2. Anabatic radon, the mean of the running diurnal composite minus background.

3. Non-anabatic radon, the daily mean minus the composite mean.

By inspecting a plot of anabatic rank vs. anabatic radon, Fig. 3, a threshold rank can be identified from when the anabatic radon concentration first reaches a minimum; day 220 in this case. Days with a rank below this threshold are defined as anabatic; the

ACPD
14, 18083–18126, 2014

others as non-anabatic. Radon concentration variability leads to scatter in the anabatic radon concentration, making it prudent to select the threshold by inspection. If the method was perfect, the anabatic radon concentration would be zero for days above the threshold, but in fact the anabatic radon concentration increases with rank for days above 220. This is a result of increasing intra-day variability combined with the method's inability to perfectly separate anabatic and non-anabatic contributions.

2.4.2 Misclassification error

As a further diagnostic we make an estimate of the false-positive error rate, expressed in terms of the average radon concentration which is mistakenly classified as being due to anabatic flows. We expect that false-positives will be present because the detection of anabatic influence relies on finding days with a diurnal radon variation which is in-phase with the composite mean. Because of random fluctuations in the timing of non-thermal mixing, some days may have an in-phase radon cycle in the absence of thermally-forced flows.

To compute the error we selectively sub-sample the observed radon time-series, obtaining a collection of days with a diurnal cycle (both individually and in composite) which is clearly due to processes other than anabatic flows. Then we apply the ranking procedure to this sub-sample of days knowing that all of the anabatic flow days in this subset are false-positives. The results from the ranking procedure, including diagnostics, are used to make an estimate of the false-positive rate on the full time-series.

The sub-sample is generated by selecting all days whose radon concentration, lagged by 12 h, is positively correlated with the composite mean; we select days which appear to have anabatic mountain winds during the night. Then, the mean daily anabatic radon concentration in the full data set which is due to misclassified non-anabatic processes is given by

ACPD
14, 18083–18126, 2014

$$a_{\mathrm{m}} = \frac{1}{N} \sum_{i=1}^{N_{\mathrm{s}}} a_{\mathrm{s}}^{(i)} \quad (1)$$

where: a_{m} is the anabatic radon concentration due to misclassification; $a_{\mathrm{s}}^{(i)}$ is the anabatic radon concentration on the ith day in the subset described above, N is the number of days in the full data set, and N_{s} is the number of days in the subset.

3 Results and discussion

3.1 Characteristics of the radon distribution

Seasonal radon composites are shown in Fig. 4, including a break-down by trajectory direction. Over the two-year period, hourly radon measurements were available for 88 % of the time, allowing 77 % of the days to be ranked for the likely presence of anabatic flows. Missing data were spread throughout the year, meaning that the data gaps do not introduce a seasonal bias.

Mean radon concentrations are sensitive to the time-of-day, season, and wind direction. Furthermore, the average strength of the diurnal cycle changes with wind direction.

Diurnal cycles are absent in winter, but present for the other seasons. For these two years, composites of months October–March (not shown) had a negligible diurnal cycle.

Radon concentrations are higher, about double, when the airmass arrives from the south-east. A partial explanation could be higher radon emissions from the south-east of the Alps, which are reported by López-Coto et al. (2013) but not evident in the results of Szegvary et al. (2009) or Manohar et al. (2013). Notwithstanding the possible influence of flux variations, a systematic difference in land-surface influence is likely. Air arriving from the south-east crosses the full width of the Alps before arriving at

ACPD
14, 18083–18126, 2014

Jungfraujoch, whereas the approach from the north-west is unobstructed. Adding to the contrast, large scale atmospheric conditions may be more favourable for vertical transport during periods of south-east flow, for instance föhn winds arrive from the south more frequently than from the north (Zellweger et al., 2003). Determining the relative importance of these factors is out of the scope of the present study, but we take wind direction direction effects into account by restricting our attention to north-west fetch in some of the analyses which follow.

Temporal radon variations result from changes in mixing and fetch, each of which vary diurnally and seasonally. Subdividing the radon observations by season, hour of day, and wind direction isolates some of the radon variability, with seasonal changes in the diurnal cycle being most obvious in Fig. 4. The remaining spread, between the 25th and 75th percentiles, indicates that a large fraction of the radon variability happens on different time-scales.

In Fig. 5 composites are generated according to the anabatic rank by grouping together days with diurnal cycles of similar strength. Although each of these composites are generated from a similar number of samples to those of Fig. 4, the diurnal cycle explains a large fraction of the concentration variance for the low rank days, as seen by the narrow spread in hourly distributions relative to the size of the diurnal peak.

To place the Jungfraujoch radon measurements in context, the observations at Bern, 3 km below on the Swiss plateau, are also shown in this plot. For the highest ranking composite, days 1–50, the daytime peak radon concentration at Jungfraujoch equals the daytime minimum value measured at Bern. This suggests that the two sites sample the same air mass on the low-rank days.

The lower ranked composites are associated with an increasing separation between Bern and Jungfraujoch until the diurnal cycle disappears from the Jungfraujoch data on about the 200th day. After this point, in the absence of a diurnal signal, the ranking algorithm sorts days from low-to-high intra-day variability. We see that days with larger variability are more likely to have higher mean values; the composite of the last days selected by the algorithm (days 511–580) is without a significant diurnal cycle, but the

ACPD
14, 18083–18126, 2014

mean radon concentration is high (1.94 Bq m^{-3} STP compared with 1.03 Bq m^{-3} STP for days 200–249). As well as having a high variability, the hourly distributions of Jungfraujoch observations overlap with the daytime minimum seen in Bern. High radon concentrations mean that these days are associated with strong vertical transport, sometimes bringing boundary-layer air to Jungfraujoch with little dilution, but the absence of a composite diurnal cycle means that vertical transport is not driven by solar forcing.

Compared with a ranking based on fitting a sinusoid to daily concentration fluctuations (Gallagher et al., 2011), our method agrees well overall. For the 100 most anabatic days, according to our method, only one was non-anabatic according to a sinusoid fit. For the days ranked 100–200 however, 27 were classified as non-anabatic by the sinusoid method. For the days which differed, those classified as anabatic by our method typically had a rapid morning increase in radon without an evening drop, consistent with an anabatic event followed by stagnation of the large-scale flow. The opposite held true for anabatic days according to the sinusoid fit, which were characterised by flat concentrations throughout the day followed by a rapid drop during the night – thus fitting a sinusoid reasonably well, despite being unlikely to result from anabatic mountain winds. In summary, our ranking method appears to perform better than the sinusoid method, but mainly when anabatic flows are weak. As a consequence, the difference between the methods is likely to be of only minor significance for the interpretation of atmospheric composition observations.

Figure 6 shows the decomposed seasonal cycle. Anabatic radon, i.e. radon arriving at Jungfraujoch as a result of thermally-forced transport, is close to the expected false-positive concentration in October through to March, meaning that thermally-driven transport is absent during these months. This is consistent with the negligible diurnal cycles we observed over this period, and in close agreement with Pandey Deolal et al. (2013), who observed weak diurnal cycles of peroxyacetyl nitrate (PAN) and reactive nitrogen species (NO_y) during these months.

ACPD
14, 18083–18126, 2014

Non-anabatic radon shows a weak seasonal cycle. While this may be a real phenomenon, associated with changes in airmass fetch, the decomposition method is only approximate, and cannot prevent a proportion of anabatic radon leaking into the non-anabatic classification. These results are therefore consistent with there being no seasonal change in vertical transport by non-anabatic flows, but a weak seasonal cycle in non-anabatic transport is also a possibility. Over these two years, the monthly mean wind speed was lower in summer, typically 5 m s^{-1} compared with 7 m s^{-1} during winter indicating, if anything, the potential for stronger non-anabatic transport in winter.

It is also possible that the apparent correspondence between the mean anabatic and non-anabatic concentrations in Fig. 6 are attributable to approximations of the method. A more reliable indicator of the importance of anabatic flows is the magnitude of the seasonal cycle; radon doubles in summer compared with winter. Neglecting seasonal changes in radon emissions, likely to be higher in summer, anabatic and non-anabatic mechanisms are therefore equally important in summer.

The monthly distributions of daily minimum radon concentration also show a seasonality, with higher concentrations in summer. A simple explanation exists if the influence of anabatic flow conditions persists through to the following day.

Figure 7 shows the multi-day composite radon concentration, constructed by selecting periods when a day with anabatic influence is followed by two days without. Data where back-trajectories indicated south-east fetch were excluded to avoid the effect of any systematic wind shifts associated with a change from anabatic to non-anabatic conditions. After an anabatic flow event, mean and median radon concentration remain elevated for up to 48 h after the anabatic peak. Though dropping rapidly from the afternoon peak, night-time radon concentrations remain elevated after an anabatic event compared with the concentration during the previous night.

3.2 Comparison with other indicators of upslope winds

Radon's physical properties and source distribution make it almost ideal as a passive tracer of land influence. On the other hand, it is not as widely observed as some other

ACPD
14, 18083–18126, 2014

tracers or aerosol parameters. In particular the water vapour mixing ratio, r, is a convenient tracer because of widespread measurements.

Figure 8 shows how radon and water vapour compare as an indicator of anabatic flow. Assuming the radon technique is accurate, anabatic flow occurs on around 40 % of days (Fig. 8a). An approach based on water vapour increases this estimate to 50 % (Fig. 8b). Two other options which we examined, the aerosol scattering coefficient and carbon monoxide concentration (Fig. 8c and d), detected roughly half as many anabatic days, whereas NO_y led to a similar proportion of anabatic days to radon (Fig. 8e) but with radon showing a little more contrast between the two classes.

We now examine our claim that radon is more representative of surface influence than r. In order to do this we take observed daily temperatures, the gridded E-OBS data (Haylock et al., 2008), and extract a contingency table of daily maximum temperature anomalies depending on the classification according to radon and moisture, shown in Fig. 9. This is an independent test of the ranking method, based on the premise that anabatic mountain winds are more common on warm days.

Rather than showing that one method is drastically better than the other, the main result from Fig. 9 is that a more accurate classification could come from combining both. For 71 % of the time, radon and r are in agreement and are associated with statistically significant changes in maximum temperature anomalies. Days classified as anabatic are warmer than average over a large part of Europe; non-anabatic days are cooler over the same region.

When the tracers disagree, there is a much weaker signal in observed temperatures. Days which have been classified as anabatic according to r but not radon are not significantly different from usual, so are probably false-positives caused by unrelated fluctuations in r.

There are fewer days when radon, but not r, leads to an anabatic classification. On these days, there is a small (statistically significant) warm region south-east of Jungfraujoch, which also happens to be a region without significant changes in temperature for other cases. This seems to rule out all of these being false-positives, though

ACPD
14, 18083–18126, 2014

it is likely that some are. On days when r fails to detect anabatic flows, confounding factors include moisture's higher background variability compared with radon, which is a result of different sinks and sources.

In contrast to the binary anabatic/non-anabatic classification, a direct comparison of rank between radon and r leads to poor agreement. In light of this, we avoid relying on the numerical rank in analyses which follow and instead focus on the classification.

Following a different approach entirely, previous investigations (Collaud Coen et al., 2011; Lugauer et al., 1998) have found that circulation pattern classifications (Huth et al., 2008) are useful for explaining the occurrence of anabatic conditions at Jungfraujoch. Many schemes have been developed (Demuzere et al., 2011; Philipp et al., 2010); for comparison with the radon-based method we selected the CAP9 scheme, a nine-class objective scheme based on mean sea level pressure in a domain centred on the Alps which is implemented by MeteoSwiss (MeteoSwiss, 2012). We used this scheme because: it has few classes, allowing for more robust statistics in our relatively short data set; and the scheme has been demonstrated to perform well in the alpine region, for precipitation (Schiemann and Frei, 2010). When compared with our radon-based classification, we found radon concentration was weakly associated with circulation type, but circulation class was not a good predictor of anabatic conditions. Similarly, Zellweger et al. (2003) found that tracer variations (NO_y, aerosol and humidity) were a better predictor of thermally-driven vertical transport than circulation classification according to the Alpine Weather Statistics.

3.3 Airmass characteristics

Considering the different measurement footprint and transport mechanisms on anabatic vs. non-anabatic days, we expect systematic differences in airmass properties. To test this idea however, we first need to account for several other effects that also influence composition. These are: total land surface influence; large scale fetch; and season.

ACPD
14, 18083–18126, 2014

To account for the total land surface influence we bin measured parameters by a proxy: radon concentration. To eliminate the effect of different large-scale fetch regions, we restrict the comparison to trajectories arriving from the north-west. Although not shown, radon measurements do indicate a difference in the mechanism of vertical transport for south-east back-trajectories; the radon concentration – and therefore land-surface influence – increases with increasing wind speed whereas the opposite trend holds for north-west back-trajectories. Anabatic days occur only for part of the year, so a direct comparison between anabatic and non-anabatic days would bias the anabatic data towards summer measurements. Therefore, we compare only the months from April through to September, when both anabatic and non-anabatic flows are detected.

Figure 10 shows that several parameters have an inflection or discontinuity at a radon concentration of around 2 Bq m^{-3} STP.

Wind speeds differ between anabatic and non-anabatic days; winds are always lower on anabatic days, and have a weak decreasing trend with increasing radon concentration. On non-anabatic days, low radon concentrations are associated with strong winds, but are similar to anabatic days for radon concentrations greater than 2 Bq m^{-3} STP. This is consistent with the anabatic and non-anabatic days being linked to different dynamical processes. On non-anabatic days, below 1.5 Bq m^{-3} STP, an increase in wind speed means stronger vertical transport due to the interaction between terrain and synoptic scale winds. To maintain radon concentrations above this threshold, it seems that low wind speeds are needed to prevent radon being diluted by the advection of clean free-tropospheric air.

On anabatic days the air is dryer, both in terms of relative humidity and, less dramatically, the water vapour mixing ratio. Non-anabatic days are likely to be close to saturation for radon concentrations of 1.5 Bq m^{-3} STP or higher, so non-anabatic vertical transport is likely to be associated with clouds, which envelope the site for about 40 % of the year (Andrews et al., 2011; Baltensperger et al., 1998).

On anabatic days, there is a clear correlation between radon (a proxy for surface contact) and aerosol abundances. In contrast, on non-anabatic days the median aerosol

ACPD
14, 18083–18126, 2014

concentration is low and only weakly dependent on radon concentration (up until 2 Bq m^{-3} STP). In this range it is also strongly skewed; the mean is influenced by a few high-concentration events. On non-anabatic days, it is possible to observe low aerosol concentrations at the same time as high radon. These cases might be associated with precipitation and aerosol washout.

Like radon, the molar ratio of total reactive nitrogen species to carbon monoxide, [NO_y]/[CO], is used as an indicator of recent land influence (Pandey Deolal et al., 2013). Though emitted in a relatively stable ratio from pollution sources, NO_y is removed faster than CO.

For high radon concentration, which are associated with arrival of anabatic flow at the mountain peak, [NO_y]/[CO] is larger on anabatic days. This suggests that closer sources might be more important on anabatic days. The difference is relatively small, however, and an alternative explanation might be that cloud processes remove NO_y more quickly on non-anabatic days than on anabatic days when clouds tend to be absent.

For higher radon concentrations, above 2.5 Bq m^{-3} STP which is the 80th percentile of the observed distribution, many of the quantities plotted in Fig. 10 are close to constant. Although this could mean that the highest radon observations are due to local emissions, these other tracers have seasonal cycles in their sources and sinks which distorts the relationship because high radon values are most common mid-summer. Accounting for the seasonal cycle in these other tracers, by applying a high-pass filter which retains fluctuations with a period of 35 d or less, the relationship between binned radon concentration and other land-surface tracers (for example CO and N_2O, not shown) continues to increase in a near-linear fashion until 5 Bq m^{-3} STP (98.5th percentile). This suggests that local sources are not a major contributor to observed radon concentrations at Jungfraujoch.

ACPD
14, 18083–18126, 2014

3.4 Radon-derived baseline

Baseline air is characterised by undisturbed background concentrations of short-lived pollutants, though the specifics of its identification depend on the reason for study, the species in question, and the measurement site. Radon provides an unambiguous method for defining baseline conditions and has been used at sites including Mauna Loa (Chambers et al., 2013), Cape Grim (Zahorowski et al., 2013) and Jungfraujoch (Xia et al., 2013).

In Fig. 11, showing all observations unlike Fig. 10, the median aerosol scattering coefficient levels out for radon concentrations below 2 Bq m^{-3} STP; for summer non-anabatic days the shoulder is present at a similar level (Fig. 10d). So baseline aerosol statistics could be computed from a radon threshold. Here we briefly discuss how this compares with other commonly-used baseline definitions and examine the effect of excluding anabatic days.

The value of 2 Bq m^{-3} STP also corresponds with the summer [NO_y]/[CO] ratio of 0.008, identified by Pandey Deolal et al. (2013) as characteristic of baseline conditions (Fig. 10e). Arguably radon has an advantage in that a constant value is more appropriate year round, whereas the destruction rate of CO varies with season. But seasonal changes in radon emissions, which are sensitive to soil moisture, and large-scale fetch means that a seasonally-varying threshold might also be preferred for radon.

The agreement between the two criteria, though indicating consistency between the tracers, is not of critical importance; any threshold is study specific and most of the plots in Fig. 10 show a continuous variation in airmass properties rather than a step change. For instance, Xia et al. (2013) used a threshold of 0.5 Bq m^{-3} ($\sim$ 0.75 Bq m^{-3} STP), further limiting recent contributions from the land surface compared with the Pandey Deolal et al. (2013) criteria and approaching the observed radon concentration in oceanic baseline air at Mace Head, a few tens of mBq m^{-3} (Biraud et al., 2000).

Figure 12 depicts monthly median values after applying several baseline definitions to the aerosol data. For some months, a 2 Bq m^{-3} STP radon threshold may be too high

ACPD
14, 18083–18126, 2014

to eliminate transient spikes from baseline values, though a trade-off exists between data availability and smoothness. Compared with a simple time-of-day filter (Andrews et al., 2011), a radon-based definition results in a smoother seasonality of baseline values while retaining a similar amount of data. In this case, the choice of baseline definition can make a non-trivial difference.

The use of a $2\,\mathrm{Bq\,m^{-3}}$ STP threshold can be further refined, either by eliminating anabatic days or by choosing a lower value. The elimination of anabatic days, combined with a threshold of $2\,\mathrm{Bq\,m^{-3}}$ STP, has only a minor effect. A peak is removed from the baseline for April 2011, implying that unusually active mountain winds were responsible for the higher radon concentration seen that month, but otherwise it is more effective, in terms of the number of observations retained, to reduce the threshold. For sufficiently low radon thresholds, the imposition of an anabatic-day criteria is redundant, since radon is usually high on anabatic days. For thresholds of 1 or $0.75\,\mathrm{Bq\,m^{-3}}$ STP, the baseline aerosol signal converges, especially during winter, despite making a relatively large difference to data availability.

From these considerations, a baseline radon threshold of $1\,\mathrm{Bq\,m^{-3}}$ STP works well for continuous aerosol measurements, but a reasonable choice could easily lie in the range 0.75–$2\,\mathrm{Bq\,m^{-3}}$ STP, depending on the desired remoteness of land surface influence.

3.5 Aerosol washout

In Sect. 3.3 we suggested that aerosol washout was responsible for some of the differences between radon and aerosol parameters during non-anabatic conditions, as did Zellweger et al. (2003) who argued that low aerosol abundance during south föhn events was due to washout. We can show this effect explicitly, after a simple transformation of the data.

ACPD
14, 18083–18126, 2014

In order to extract the washout signal, we compute a parameter which we call the radon-normalised aerosol excess

$$a_n = \frac{a_s - \tilde{a}_s}{\mathrm{Rn} - \mathrm{Rn}_t} \quad (2)$$

where a_s is the hourly average aerosol scattering coefficient at 450 nm, $\tilde{a}_s$ is the monthly baseline of a_s, Rn is the hourly radon concentration, and $\mathrm{Rn}_t = 1\,\mathrm{Bq\,m^{-3}}$ STP is the radon threshold used for computing a_s. This is intended to represent the difference between the observed aerosol and the free-tropospheric baseline, likely to be aerosols emitted recently at the surface, normalised by the total amount of recent land surface contact.

In Fig. 13, a_n is binned according to the average rain rate along the 72 h back-trajectory. Clearly, and consistent with the action of wet removal processes, the normalised aerosol excess drops steeply with rainfall. Moderate rain rates do not necessarily mean that aerosol concentrations drop to zero but, since the timing of rainfall along the trajectory is not taken into account, this could be due to the different effect of recent rainfall compared with rainfall earlier along the trajectory. Rainfall timing can also help to explain the difference in the plots between anabatic and non-anabatic days; because anabatic days are associated with clear skies and with recent vertical transport then rainfall must have occurred earlier. On anabatic days there is time for the airmass to gather aerosols, post rainfall, before being transported upwards by the mountain wind system.

From the data in these plots, it appears that the addition of radon to a comprehensive aerosol model might help to constrain the parameterisation of aerosol washout. Furthermore, because of the difference seen between anabatic and non-anabatic conditions, consideration should be given to the vertical mixing process when interpreting the observations.

ACPD
14, 18083–18126, 2014

4 Conclusions

Radon – to a good approximation – is a direct indicator of land influence. From our analysis of the 2010–2011 hourly radon concentration at Jungfraujoch, the primary outcome was a classification of each day as affected, or unaffected, by thermally-driven (anabatic) mountain winds as well as a less-robust measure of how strong the influence was. On the most strongly affected days, matching radon concentrations at Bern and Jungfraujoch were taken as evidence of relatively unperturbed transport of boundary-layer air from the plateau to Jungfraujoch.

Anabatic winds are likely to be most prominent during conditions of clear skies and low winds. We found that anabatic days had, on average, higher daily maximum temperatures over central Europe, lower winds at Jungfraujoch, and weaker wet scavenging of aerosols. The effect on temperature was stronger when absolute humidity was used in addition to radon for classification, indicating that a more robust classification is achieved when using more than one tracer.

During periods of high relative humidity and strong winds at Jungfraujoch, high radon concentrations were sometimes observed, indicative of strong or recent land influence. However, these conditions were most likely the result of dynamic influences (e.g. föhn winds), resulting in classification as non-anabatic.

For defining the baseline aerosol scattering coefficient, i.e. the unperturbed free-tropospheric background, we showed that a radon threshold in the range of 1–2 $\mathrm{Bq\,m^{-3}}$ STP is appropriate and that the monthly background is relatively insensitive to the radon threshold within this range. Refining the definition by excluding anabatic days was of no additional benefit.

In contrast to the baseline definition, we found that our estimate of aerosol washout was affected by anabatic winds. When viewed in conjunction with the difference in airmass properties on anabatic and non-anabatic days, this is a strong incentive to take anabatic flows into account during process studies or when using Jungfraujoch measurements for emissions estimates.

ACPD
14, 18083–18126, 2014

With the continuing operation of the Jungfraujoch radon detector, which provides sensitive and quantitative measurements of the radon concentration, we anticipate that these data will be useful in other observational and modelling studies. Future studies could examine the effect of spatially and temporally varying radon emissions, overcoming one limitation of the present investigation. Instructions for accessing the radon data are at http://www.radon.unibas.ch/.

Acknowledgements. We acknowledge the E-OBS dataset from the EU-FP6 project ENSEMBLES (http://ensembles-eu.metoffice.com) and the data providers in the ECA&D project (http://www.ecad.eu); chemical and meteorological data from the World Data Centre for Greenhouse Gases (http://ds.data.jma.go.jp) and EBAS (http://ebas.nilu.no/), in particular measurements performed by Empa; and weather type classifications provided by MeteoSwiss. We thank the International Foundation High Alpine Research Stations Jungfraujoch and Gornergrat (HFSJG) for making it possible for us to carry out our measurements at the High Alpine Research Station Jungfraujoch. We are grateful to Markus Leuenberger and Peter Nyfeler from the Climate and Environmental Physics Division, Physics Institute, University of Bern, for hosting and supporting maintenance of our detector in Bern.

References

Andrews, E., Ogren, J., Bonasoni, P., Marinoni, A., Cuevas, E., Rodríguez, S., Sun, J., Jaffe, D., Fischer, E., Baltensperger, U., Weingartner, E., Coen, M. C., Sharma, S., Macdonald, A., Leaitch, W., Lin, N.-H., Laj, P., Arsov, T., Kalapov, I., Jefferson, A., and Sheridan, P.: Climatology of aerosol radiative properties in the free troposphere, Atmos. Res., 102, 365–393, doi:10.1016/j.atmosres.2011.08.017, 2011. 18087, 18099, 18102, 18125

ARL: HYSPLIT – Hybrid Single Particle Lagrangian Integrated Trajectory model, available at: http://www.arl.noaa.gov/HYSPLIT_info.php (last access: 27 March 2013), 2013. 18090

Baltensperger, U., Schwikowski, M., Jost, D., Nyeki, S., Gäggeler, H., and Poulida, O.: Scavenging of atmospheric constituents in mixed phase clouds at the high-alpine site Jungfraujoch part I: Basic concept and aerosol scavenging by clouds, Atmos. Environ., 32, 3975–3983, doi:10.1016/S1352-2310(98)00051-X, 1998. 18099

ACPD
14, 18083–18126, 2014

Balzani Lööv, J. M., Henne, S., Legreid, G., Staehelin, J., Reimann, S., Prévôt, A. S. H., Steinbacher, M., and Vollmer, M. K.: Estimation of background concentrations of trace gases at the Swiss Alpine site Jungfraujoch (3580 m a.s.l.), J. Geophys. Res., 113, D22305, doi:10.1029/2007JD009751, 2008. 18086

Biraud, S., Ciais, P., Ramonet, M., Simmonds, P., Kazan, V., Monfray, P., O'Doherty, S., Spain, T. G., and Jennings, S. G.: European greenhouse gas emissions estimated from continuous atmospheric measurements and radon 222 at Mace Head, Ireland, J. Geophys. Res., 105, 1351–1366, doi:10.1029/1999JD900821, 2000. 18101

Calvert, J. G.: Glossary of atmospheric chemistry terms (Recommendations 1990), Pure Appl. Chem., 62, 2167–2219, doi:10.1351/pac199062112167, 1990. 18084

Campana, M., Li, Y., Staehelin, J., Prevot, A. S., Bonasoni, P., Loetscher, H., and Peter, T.: The influence of south foehn on the ozone mixing ratios at the high alpine site Arosa, Atmos. Environ., 39, 2945–2955, doi:10.1016/j.atmosenv.2005.01.037, 2005. 18086

Chambers, S., Williams, A. G., Zahorowski, W., Griffiths, A., and Crawford, J.: Separating remote fetch and local mixing influences on vertical radon measurements in the lower atmosphere, Tellus B, 63, 843–859, doi:10.1111/j.1600-0889.2011.00565.x, 2011. 18087, 18089

Chambers, S. D., Zahorowski, W., Williams, A. G., Crawford, J., and Griffiths, A. D.: Identifying tropospheric baseline air masses at Mauna Loa Observatory between 2004 and 2010 using Radon-222 and back trajectories, J. Geophys. Res.-Atmos., 118, 992–1004, doi:10.1029/2012JD018212, 2013. 18101

Chevillard, A., Ciais, P., Karstens, U., Heimann, M., Schmidt, M., Levin, I., Jacob, D., Podzun, R., Kazan, V., Sartorius, H., and Weingartner, E.: Transport of ^{222}Rn using the regional model REMO: a detailed comparison with measurements over Europe, Tellus B, 54, 850–871, doi:10.1034/j.1600-0889.2002.01339.x, 2002. 18087

Collaud Coen, M., Weingartner, E., Furger, M., Nyeki, S., Prévôt, A. S. H., Steinbacher, M., and Baltensperger, U.: Aerosol climatology and planetary boundary influence at the Jungfraujoch analyzed by synoptic weather types, Atmos. Chem. Phys., 11, 5931–5944, doi:10.5194/acp-11-5931-2011, 2011. 18085, 18086, 18087, 18098

Cui, J., Deolal, S. P., Sprenger, M., Henne, S., Staehelin, J., Steinbacher, M., and Nédélec, P.: Free tropospheric ozone changes over Europe as observed at Jungfraujoch (1990–2008): an analysis based on backward trajectories, J. Geophys. Res., 116, D10304, doi:10.1029/2010JD015154, 2011. 18086

ACPD
14, 18083–18126, 2014

De Wekker, S. F. J., Steyn, D. G., and Nyeki, S.: A comparison of aerosol-layer and convective boundary-layer structure over a mountain range during STAAARTE '97, Bound.-Lay. Meteorol., 113, 249–271, doi:10.1023/B:BOUN.0000039371.41823.37, 2004. 18085

Demuzere, M., Kassomenos, P., and Philipp, A.: The COST733 circulation type classification software: an example for surface ozone concentrations in Central Europe, Theor. Appl. Climatol., 105, 143–166, doi:10.1007/s00704-010-0378-4, 2011. 18098

Draxler, R. and Hess, G.: Description of the HYSPLIT-4 Modeling System, Tech. Rep. ARL-224, NOAA, Silver Spring, Maryland, 1998. 18089

Drobinski, P., Steinacker, R., Richner, H., Baumann-Stanzer, K., Beffrey, G., Benech, B., Berger, H., Chimani, B., Dabas, A., Dorninger, M., Dürr, B., Flamant, C., Frioud, M., Furger, M., Gröhn, I., Gubser, S., Gutermann, T., Häberli, C., Häller-Scharnhost, E., Jaubert, G., Lothon, M., Mitev, V., Pechinger, U., Piringer, M., Ratheiser, M., Ruffieux, D., Seiz, G., Spatzierer, M., Tschannett, S., Vogt, S., Werner, R., and Zängl, G.: Föhn in the Rhine Valley during MAP: a review of its multiscale dynamics in complex valley geometry, Q. J. Roy. Meteor. Soc., 133, 897–916, doi:10.1002/qj.70, 2007. 18086

Feichter, J. and Crutzen, P. J.: Parameterization of vertical tracer transport due to deep cumulus convection in a global transport model and its evaluation with ^{222}Radon measurements, Tellus B, 42, 100–117, doi:10.1034/j.1600-0889.1990.00011.x, 1990. 18088

Folini, D., Ubl, S., and Kaufmann, P.: Lagrangian particle dispersion modeling for the high Alpine site Jungfraujoch, J. Geophys. Res., 113, D18111, doi:10.1029/2007JD009558, 2008. 18090

Forrer, J., Rüttimann, R., Schneiter, D., Fischer, A., Buchmann, B., and Hofer, P.: Variability of trace gases at the high-Alpine site Jungfraujoch caused by meteorological transport processes, J. Geophys. Res.-Atmos., 105, 12241–12251, doi:10.1029/1999JD901178, 2000. 18085

Furger, M.: The radiosoundings of Payerne: Aspects of the synoptic-dynamic climatology of the wind field near mountain ranges, Theor. Appl. Climatol., 45, 3–17, doi:10.1007/BF00865989, 1992. 18085

Gallagher, J. P., McKendry, I. G., Macdonald, A. M., and Leaitch, W. R.: Seasonal and diurnal variations in aerosol concentration on Whistler Mountain: boundary layer influence and synoptic-scale controls, J. Appl. Meteorol. Climatol., 50, 2210–2222, doi:10.1175/JAMC-D-11-028.1, 2011. 18090, 18095

Gallagher, J. P., McKendry, I. G., Cottle, P. W., Macdonald, A. M., Leaitch, W. R., and Strawbridge, K.: Application of lidar data to assist airmass discrimination at the Whistler Moun-

ACPD
14, 18083–18126, 2014

taintop Observatory, J. Appl. Meteorol. Climatol., 51, 1733–1739, doi:10.1175/JAMC-D-12-067.1, 2012. 18087
Griffiths, A. D., Parkes, S. D., Chambers, S. D., McCabe, M. F., and Williams, A. G.: Improved mixing height monitoring through a combination of lidar and radon measurements, Atmos. Meas. Tech., 6, 207–218, doi:10.5194/amt-6-207-2013, 2013. 18087
Grossi, C., Arnold, D., Adame, J., López-Coto, I., Bolívar, J., de la Morena, B., and Vargas, A.: Atmospheric ^{222}Rn concentration and source term at *El Arenosillo* 100 m meteorological tower in southwest Spain, Radiat. Meas., 47, 149–162, doi:10.1016/j.radmeas.2011.11.006, 2012. 18087
Guedalia, D., Lopez, A., Fontan, J., and Birot, A.: Aircraft Measurements of Rn-222, Aitken Nuclei and Small Ions up to 6 km, J. Appl. Meteorol., 11, 357–365, doi:10.1175/1520-0450(1972)011<0357:AMORAN>2.0.CO;2, 1972. 18087
Haiden, T.: On the pressure field in the slope wind layer, J. Atmos. Sci., 60, 1632–1635, doi:10.1175/1520-0469(2003)60<1632:OTPFIT>2.0.CO;2, 2003. 18086
Haylock, M. R., Hofstra, N., Klein Tank, A. M. G., Klok, E. J., Jones, P. D., and New, M.: A European daily high-resolution gridded data set of surface temperature and precipitation for 1950–2006, J. Geophys. Res., 113, D20119, doi:10.1029/2008JD010201, 2008. 18097, 18122
Henne, S., Furger, M., Nyeki, S., Steinbacher, M., Neininger, B., de Wekker, S. F. J., Dommen, J., Spichtinger, N., Stohl, A., and Prévôt, A. S. H.: Quantification of topographic venting of boundary layer air to the free troposphere, Atmos. Chem. Phys., 4, 497–509, doi:10.5194/acp-4-497-2004, 2004. 18085, 18086
Henne, S., Furger, M., and Prévôt, A. S. H.: Climatology of mountain venting-induced elevated moisture layers in the lee of the Alps, J. Appl. Meteorol., 44, 620–633, doi:10.1175/JAM2217.1, 2005. 18085, 18086
Huth, R., Beck, C., Philipp, A., Demuzere, M., Ustrnul, Z., Cahynová, M., Kyselý, J., and Tveito, O. E.: Classifications of atmospheric circulation patterns, Ann. N. Y. Acad. Sci., 1146, 105–152, doi:10.1196/annals.1446.019, 2008. 18098
Keeling, C. D., Bacastow, R. B., Bainbridge, A. E., Ekdahl, C. A., Guenther, P. R., Waterman, L. S., and Chin, J. F. S.: Atmospheric carbon dioxide variations at Mauna Loa Observatory, Hawaii, Tellus, 28, 538–551, doi:10.1111/j.2153-3490.1976.tb00701.x, 1976. 18084
Ketterer, C., Zieger, P., Bukowiecki, N., Collaud Coen, M., Maier, O., Ruffieux, D., and Weingartner, E.: Investigation of the planetary boundary layer in the Swiss Alps using remote sensing

ACPD
14, 18083–18126, 2014

and in situ measurements, Bound.-Lay. Meteorol., 151, 317–334, doi:10.1007/s10546-013-9897-8, 2014. 18085, 18087

Kossmann, M., Corsmeier, U., De Wekker, S., Fiedler, F., Vögtlin, R., Kalthoff, N., Güsten, H., and Neininger, B.: Observations of handover processes between the atmospheric boundary layer and the free troposphere over mountainous terrain, Contrib. Atmos. Phys., 72, 329–350, 1999. 18085, 18086

Lee, H. N. and Cicerone, R. J.: Vertical Diffusion in the Lower Atmosphere Using Aircraft Measurements of ^{222}Rn, J. Appl. Meteorol., 36, 1262–1270, doi:10.1175/1520-0450(1997)036<1262:VDITLA>2.0.CO;2, 1997. 18087

López-Coto, I., Mas, J., and Bolivar, J.: A 40-year retrospective European radon flux inventory including climatological variability, Atmos. Environ., 73, 22–33, doi:10.1016/j.atmosenv.2013.02.043, 2013. 18093

Lothon, M., Druilhet, A., Bénech, B., Campistron, B., Bernard, S., and Saïd, F.: Experimental study of five föhn events during the Mesoscale Alpine Programme: From synoptic scale to turbulence, Q. J. Roy. Meteor. Soc., 129, 2171–2193, doi:10.1256/qj.02.30, 2003. 18086

Lugauer, M., Baltensperger, U., Furger, M., Gäggeler, H. W., Jost, D. T., Schwikowski, M., and Wanner, H.: Aerosol transport to the high Alpine sites Jungfraujoch (3454 m a.s.l.) and Colle Gnifetti (4452 m a.s.l.), Tellus B, 50, 76–92, doi:10.1034/j.1600-0889.1998.00006.x, 1998. 18085, 18098

Lugauer, M., Baltensperger, U., Furger, M., Gäggeler, H. W., Jost, D. T., Nyeki, S., and Schwikowski, M.: Influences of vertical transport and scavenging on aerosol particle surface area and radon decay product concentrations at the Jungfraujoch (3454 m above sea level), J. Geophys. Res., 105, 19869–19879, doi:10.1029/2000JD900184, 2000. 18087

Mahrt, L.: Momentum balance of gravity flows, J. Atmos. Sci., 39, 2701–2711, doi:10.1175/1520-0469(1982)039<2701:MBOGF>2.0.CO;2, 1982. 18086

Manohar, S., Meijer, H., and Herber, M.: Radon flux maps for the Netherlands and Europe using terrestrial gamma radiation derived from soil radionuclides, Atmos. Environ., 81, 399–412, doi:10.1016/j.atmosenv.2013.09.005, 2013. 18093

MeteoSwiss: Weather type classifications, available at: http://www.meteoswiss.admin.ch/web/en/services/data_portal/standard_products/Weather_type_class.html (last access: 4 October 2012), 2012. 18098

NILU: EBAS, available at: http://ebas.nilu.no/ (last access: 12 August 2012), 2012. 18089

ACPD
14, 18083–18126, 2014

Nyeki, S., Kalberer, M., Colbeck, I., Wekker, S. D., Furger, M., Gäggeler, H. W., Kossmann, M., Lugauer, M., Steyn, D., Weingartner, E., Wirth, M., and Baltensperger, U.: Convective boundary layer evolution to 4 km a.s.l. over high-Alpine terrain: airborne lidar observations in the Alps, Geophys. Res. Lett., 27, 689–692, doi:10.1029/1999GL010928, 2000. 18086, 18087

Pandey Deolal, S., Staehelin, J., Brunner, D., Cui, J., Steinbacher, M., Zellweger, C., Henne, S., and Vollmer, M. K.: Transport of PAN and NO_y from different source regions to the Swiss high alpine site Jungfraujoch, Atmos. Environ., 64, 103–115, doi:10.1016/j.atmosenv.2012.08.021, 2013. 18095, 18100, 18101, 18125

Philipp, A., Bartholy, J., Beck, C., Erpicum, M., Esteban, P., Fettweis, X., Huth, R., James, P., Jourdain, S., Kreienkamp, F., Krennert, T., Lykoudis, S., Michalides, S. C., Pianko-Kluczynska, K., Post, P., Álvarez, D. R., Schiemann, R., Spekat, A., and Tymvios, F. S.: Cost733cat – a database of weather and circulation type classifications, Phys. Chem. Earth, 35, 360–373, doi:10.1016/j.pce.2009.12.010, 2010. 18098

Pourchet, M., Richon, P., and Sabroux, J. C.: Lead-210 and radon-222 anomalies in Mont Blanc snow, French Alps, J. Environ. Radioact., 48, 349–357, doi:10.1016/S0265-931X(99)00084-3, 2000. 18087

Prévôt, A. S., Dommen, J., and Bäumle, M.: Influence of road traffic on volatile organic compound concentrations in and above a deep Alpine valley, Atmos. Environ., 34, 4719–4726, doi:10.1016/S1352-2310(00)00254-5, 2000. 18086, 18090

Purvis, R. M., Lewis, A. C., Carney, R. A., McQuaid, J. B., Arnold, S. R., Methven, J., Barjat, H., Dewey, K., Kent, J., Monks, P. S., Carpenter, L. J., Brough, N., Penkett, S. A., and Reeves, C. E.: Rapid uplift of nonmethane hydrocarbons in a cold front over central Europe, J. Geophys. Res.-Atmos., 108, 4224, doi:10.1029/2002JD002521, 2003. 18086

Reimann, S., Schaub, D., Stemmler, K., Folini, D., Hill, M., Hofer, P., Buchmann, B., Simmonds, P. G., Greally, B. R., and O'Doherty, S.: Halogenated greenhouse gases at the Swiss High Alpine Site of Jungfraujoch (3580 m a.s.l.): continuous measurements and their use for regional European source allocation, J. Geophys. Res.-Atmos., 109, D05307, doi:10.1029/2003JD003923, 2004. 18085

Reimann, S., Vollmer, M., Folini, D., Steinbacher, M., Hill, M., Buchmann, B., Zander, R., and Mahieu, E.: Observations of long-lived anthropogenic halocarbons at the high-Alpine site of Jungfraujoch (Switzerland) for assessment of trends and European sources, Sci. Total Environ., 391, 224–231, doi:10.1016/j.scitotenv.2007.10.022, 2008. 18085

ACPD
14, 18083–18126, 2014

Rotach, M. W. and Zardi, D.: On the boundary-layer structure over highly complex terrain: Key findings from MAP, Q. J. Roy. Meteor. Soc., 133, 937–948, doi:10.1002/qj.71, 2007. 18084

Schiemann, R. and Frei, C.: How to quantify the resolution of surface climate by circulation types: an example for Alpine precipitation, Phys. Chem. Earth, 35, 403–410, doi:10.1016/j.pce.2009.09.005, 2010. 18098

Seibert, P., Kromp-kolb, H., Kasper, A., Kalina, M., Puxbaum, H., Jost, D. T., Schwikowski, M., and Baltensperger, U.: Transport of polluted boundary layer air from the Po Valley to high-alpine sites, Atmos. Environ., 32, 3953–3965, doi:10.1016/S1352-2310(97)00174-X, 1998. 18085

Stohl, A., Spichtinger-Rakowsky, N., Bonasoni, P., Feldmann, H., Memmesheimer, M., Scheel, H. E., Trickl, T., Hübener, S., Ringer, W., and Mandl, M.: The influence of stratospheric intrusions on alpine ozone concentrations, Atmos. Environ., 34, 1323–1354, doi:10.1016/S1352-2310(99)00320-9, 2000. 18085

Stohl, A., Seibert, P., Arduini, J., Eckhardt, S., Fraser, P., Greally, B. R., Lunder, C., Maione, M., Mühle, J., O'Doherty, S., Prinn, R. G., Reimann, S., Saito, T., Schmidbauer, N., Simmonds, P. G., Vollmer, M. K., Weiss, R. F., and Yokouchi, Y.: An analytical inversion method for determining regional and global emissions of greenhouse gases: Sensitivity studies and application to halocarbons, Atmos. Chem. Phys., 9, 1597–1620, doi:10.5194/acp-9-1597-2009, 2009. 18085

Szegvary, T., Leuenberger, M. C., and Conen, F.: Predicting terrestrial ^{222}Rn flux using gamma dose rate as a proxy, Atmos. Chem. Phys., 7, 2789–2795, doi:10.5194/acp-7-2789-2007, 2007. 18087

Szegvary, T., Conen, F., and Ciais, P.: European ^{222}Rn inventory for applied atmospheric studies, Atmos. Environ., 43, 1536–1539, doi:10.1016/j.atmosenv.2008.11.025, 2009. 18093

Trickl, T., Feldmann, H., Kanter, H.-J., Scheel, H.-E., Sprenger, M., Stohl, A., and Wernli, H.: Forecasted deep stratospheric intrusions over Central Europe: case studies and climatologies, Atmos. Chem. Phys., 10, 499–524, doi:10.5194/acp-10-499-2010, 2010. 18085

Uglietti, C., Leuenberger, M., and Brunner, D.: European source and sink areas of CO_2 retrieved from Lagrangian transport model interpretation of combined O_2 and CO_2 measurements at the high alpine research station Jungfraujoch, Atmos. Chem. Phys., 11, 8017–8036, doi:10.5194/acp-11-8017-2011, 2011. 18085

Vogel, F. R., Thiruchittampalam, B., Theloke, J., Kretschmer, R., Gerbig, C., Hammer, S., and Levin, I.: Can we evaluate a fine-grained emission model using high-resolution atmo-

ACPD
14, 18083–18126, 2014

spheric transport modelling and regional fossil fuel CO_2 observations?, Tellus B, 65, 18681, doi:10.3402/tellusb.v65i0.18681, 2013. 18088
Weigel, A. P., Chow, F. K., and Rotach, M. W.: The effect of mountainous topography on moisture exchange between the "surface" and the free atmosphere, Bound.-Lay. Meteorol., 125, 227–244, doi:10.1007/s10546-006-9120-2, 2006. 18085, 18086
Weiss-Penzias, P., Jaffe, D. A., Swartzendruber, P., Dennison, J. B., Chand, D., Hafner, W., and Prestbo, E.: Observations of Asian air pollution in the free troposphere at Mount Bachelor Observatory during the spring of 2004, J. Geophys. Res.-Atmos., 111, D10304, doi:10.1029/2005JD006522, 2006. 18087
Weissmann, M., Braun, F. J., Gantner, L., Mayr, G. J., Rahm, S., and Reitebuch, O.: The Alpine mountain–plain circulation: airborne doppler lidar measurements and numerical simulations, Mon. Weather Rev., 133, 3095–3109, doi:10.1175/MWR3012.1, 2005. 18084, 18086
Whittlestone, S. and Zahorowski, W.: Baseline radon detectors for shipboard use: development and deployment in the First Aerosol Characterization Experiment (ACE 1), J. Geophys. Res., 103, 16743–16751, doi:10.1029/98JD00687, 1998. 18088
Williams, A. G., Zahorowski, W., Chambers, S., Griffiths, A., Hacker, J. M., Element, A., and Werczynski, S.: The vertical distribution of radon in clear and cloudy daytime terrestrial boundary layers, J. Atmos. Sci., 68, 155–174, doi:10.1175/2010JAS3576.1, 2011. 18087
Williams, A. G., Chambers, S., and Griffiths, A.: Bulk mixing and decoupling of the nocturnal stable boundary layer characterized using a ubiquitous natural tracer, Bound.-Lay. Meteorol., 149, 381–402, doi:10.1007/s10546-013-9849-3, 2013. 18087
WMO: World Data Centre for Greenhouse Gases (WDCGG), available at: http://ds.data.jma.go.jp/gmd/wdcgg/ (last access: 1 October 2012), 2012. 18089
Xia, Y., Sartorius, H., Schlosser, C., Stöhlker, U., Conen, F., and Zahorowski, W.: Comparison of one- and two-filter detectors for atmospheric ^{222}Rn measurements under various meteorological conditions, Atmos. Meas. Tech., 3, 723–731, doi:10.5194/amt-3-723-2010, 2010. 18088
Xia, Y., Conen, F., and Alewell, C.: Total bacterial number concentration in free tropospheric air above the Alps, Aerobiologia, 29, 153–159, doi:10.1007/s10453-012-9259-x, 2013. 18101
Yamazawa, H., Miyazaki, T., Moriizumi, J., Iida, T., Takeda, S., Nagara, S., Sato, K., and Tokizawa, T.: Radon exhalation from a ground surface during a cold snow season, Int. Congr. Ser., 1276, 221–222, doi:10.1016/j.ics.2004.11.153, 2005. 18087

ACPD
14, 18083–18126, 2014

Zahorowski, W., Chambers, S., and Henderson-Sellers, A.: Ground based radon-222 observations and their application to atmospheric studies, J. Environ. Radioact., 76, 3–33, doi:10.1016/j.jenvrad.2004.03.033, 2004. 18088

Zahorowski, W., Griffiths, A. D., Chambers, S. D., Williams, A. G., Law, R. M., Crawford, J., and Werczynski, S.: Constraining annual and seasonal radon-222 flux density from the Southern Ocean using radon-222 concentrations in the boundary layer at Cape Grim, Tellus B, 65, 19622, 2013. 18101

Zardi, D. and Whiteman, C. D.: Diurnal mountain wind systems, in: Mountain Weather Research and Forecasting, edited by: Chow, F. K., Wekker, S. F. J. D., and Snyder, B. J., Springer Atmospheric Sciences, 35–119, Springer Netherlands, 2013. 18084

Zellweger, C., Ammann, M., Buchmann, B., Hofer, P., Lugauer, M., Rüttimann, R., Streit, N., Weingartner, E., and Baltensperger, U.: Summertime NO_y speciation at the Jungfraujoch, 3580 m above sea level, Switzerland, J. Geophys. Res.-Atmos., 105, 6655–6667, doi:10.1029/1999JD901126, 2000. 18085

Zellweger, C., Forrer, J., Hofer, P., Nyeki, S., Schwarzenbach, B., Weingartner, E., Ammann, M., and Baltensperger, U.: Partitioning of reactive nitrogen (NO_y) and dependence on meteorological conditions in the lower free troposphere, Atmos. Chem. Phys., 3, 779–796, doi:10.5194/acp-3-779-2003, 2003. 18085, 18087, 18094, 18098, 18102

Zhang, K., Wan, H., Zhang, M., and Wang, B.: Evaluation of the atmospheric transport in a GCM using radon measurements: sensitivity to cumulus convection parameterization, Atmos. Chem. Phys., 8, 2811–2832, doi:10.5194/acp-8-2811-2008, 2008. 18088

Zhang, K., Feichter, J., Kazil, J., Wan, H., Zhuo, W., Griffiths, A. D., Sartorius, H., Zahorowski, W., Ramonet, M., Schmidt, M., Yver, C., Neubert, R. E. M., and Brunke, E.-G.: Radon activity in the lower troposphere and its impact on ionization rate: a global estimate using different radon emissions, Atmos. Chem. Phys., 11, 7817–7838, doi:10.5194/acp-11-7817-2011, 2011. 18087

ACPD
14, 18083–18126, 2014

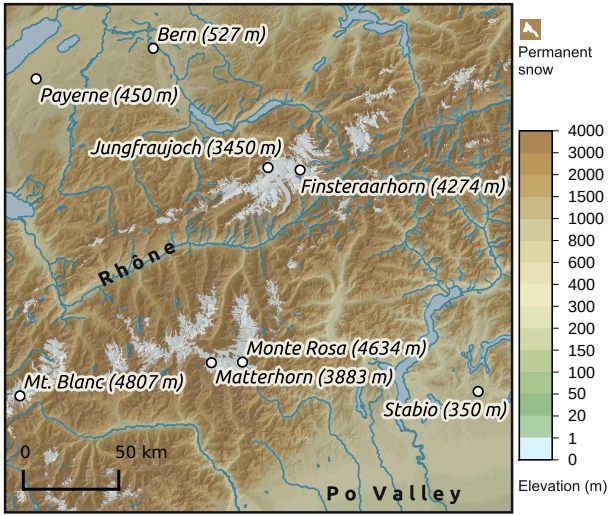

Figure 1. Jungfraujoch region. Radon detectors are installed at Jungfraujoch and Bern, separated horizontally by 61 km. Water vapour and CO are measured at Jungfraujoch and Payerne.

ACPD
14, 18083–18126, 2014

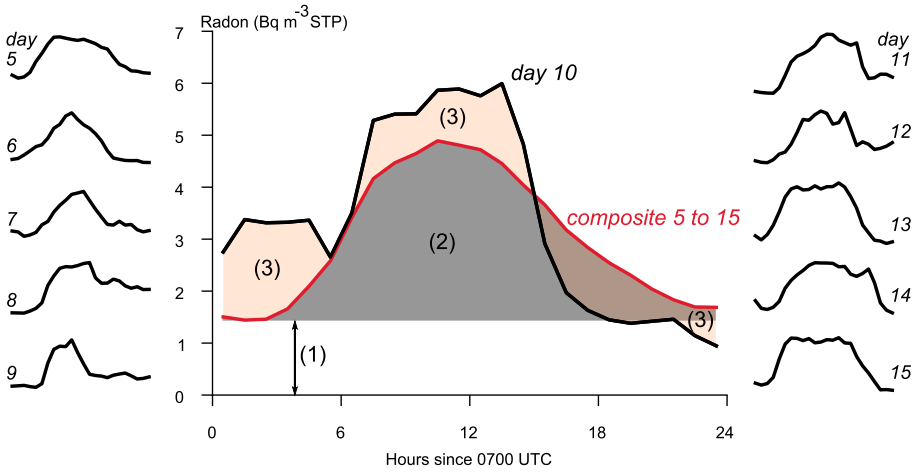

Figure 2. The definition of diagnostic quantities computed after ranking days by their contribution to the radon diurnal composite, termed the anabatic rank. Diagnostics for the *i*th day, day 10 in this example, are computed from the *i*th day radon concentration and the composite of days ranked from $i-5$ to $i+5$. These are: (1) baseline, the minimum of the composite; (2) anabatic; the mean of the composite; and (3) non-anabatic, the mean of the *i*th day minus the mean of the composite.

ACPD
14, 18083–18126, 2014

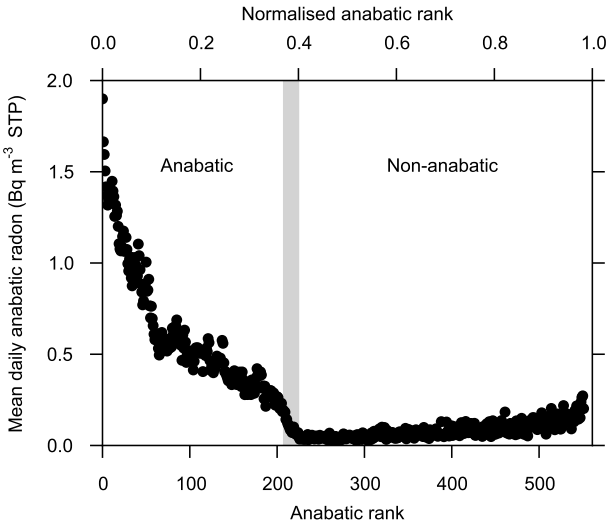

Figure 3. The daily mean anabatic radon concentration as a function of anabatic rank. Days with a rank above 220 (when the anabatic radon concentration first reaches its minimum) have a diurnal radon variation which is uncharacteristic of anabatic flows and are classified as non-anabatic.

ACPD
14, 18083–18126, 2014

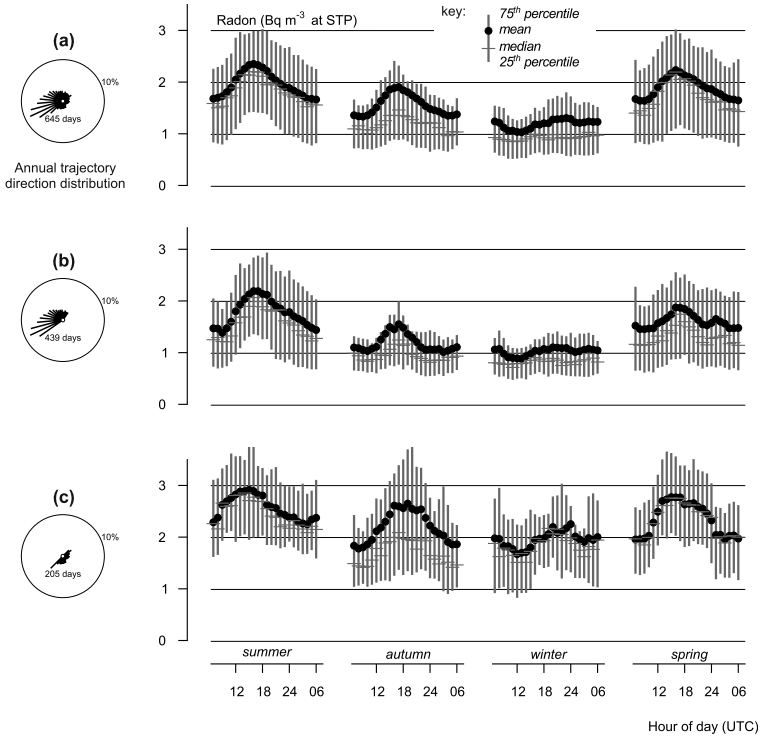

Figure 4. Radon diurnal and seasonal cycle. The plots show the mean of each bin (dot), median (horizontal bar) and the 25–75th percentile range (vertical bar). The synoptic-scale wind direction is calculated from the back-trajectory position at a distance of 61 km (the distance between Bern and Jungfraujoch). **(a)** show all directions, **(b)** show air arriving from the north-western side of the Alps (which are aligned south-west to north-east), and **(c)** show air arriving from the south-east after passing over the full width of the Alps.

ACPD
14, 18083–18126, 2014

Surface-to-mountaintop transport at the Jungfraujoch

A. D. Griffiths et al.

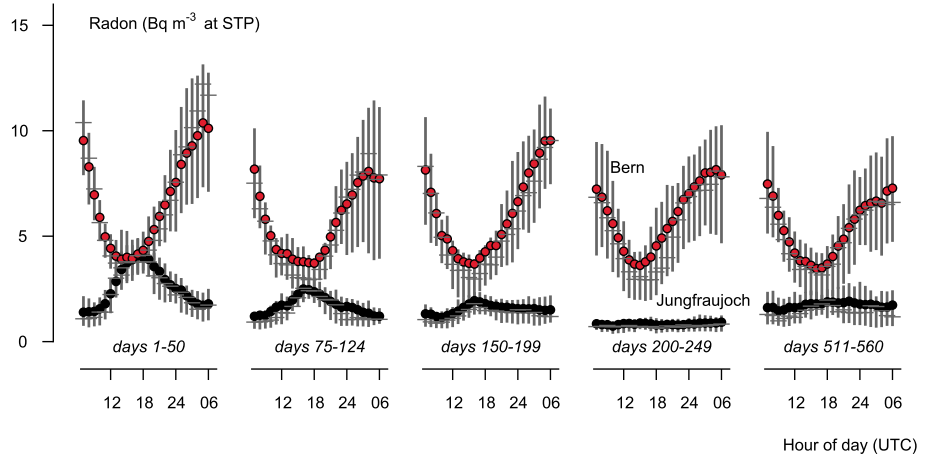

Figure 5. Fifty day diurnal composite radon concentration by anabatic rank. The airmass is fully mixed between Bern and Jungfraujoch during the afternoon on days with a rank of 50 or less; days with a rank of 200 or more are considered to be unaffected by anabatic winds. The symbols have the same meaning as Fig. 4.

ACPD
14, 18083–18126, 2014

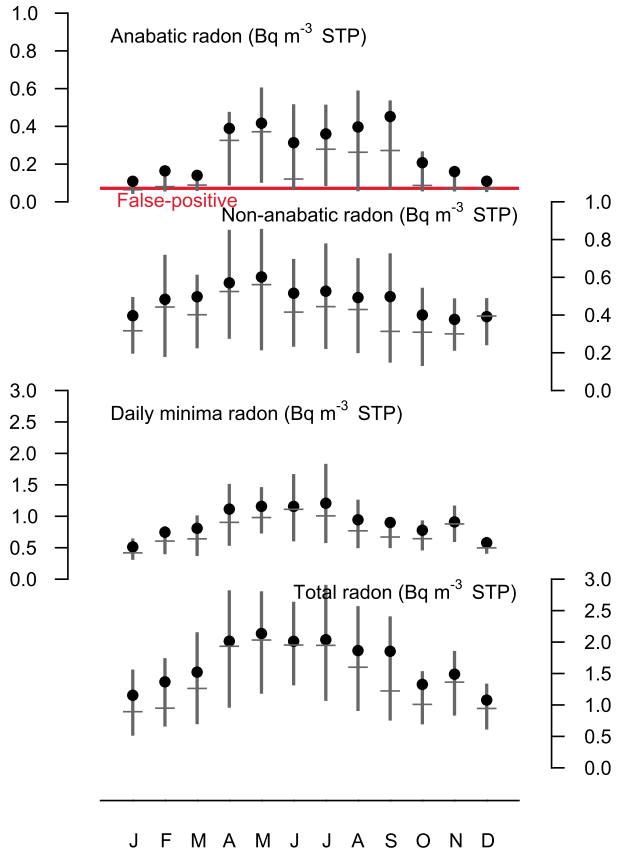

Figure 6. Seasonal cycle of decomposed daily radon concentration using the definitions shown in Fig. 2. The annual mean false-positive contribution is included on the anabatic plot, showing that anabatic flows are detected with confidence during the months of April–September. The symbols have the same meaning as Fig. 4.

ACPD
14, 18083–18126, 2014

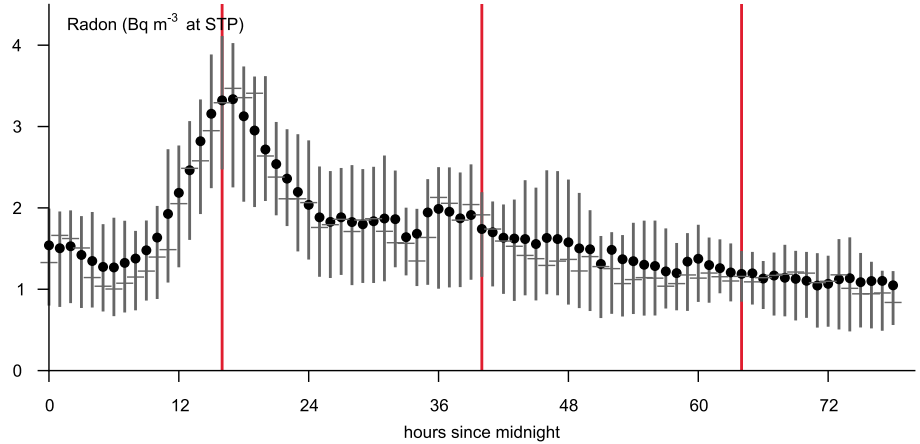

Figure 7. Three day radon composites (~ 19 samples per bin) of anabatic followed by two non-anabatic days, selecting north-west fetch. Red lines show the median peak radon concentration, 24 h after, and 48 h after. The symbols have the same meaning as Fig. 4.

ACPD
14, 18083–18126, 2014

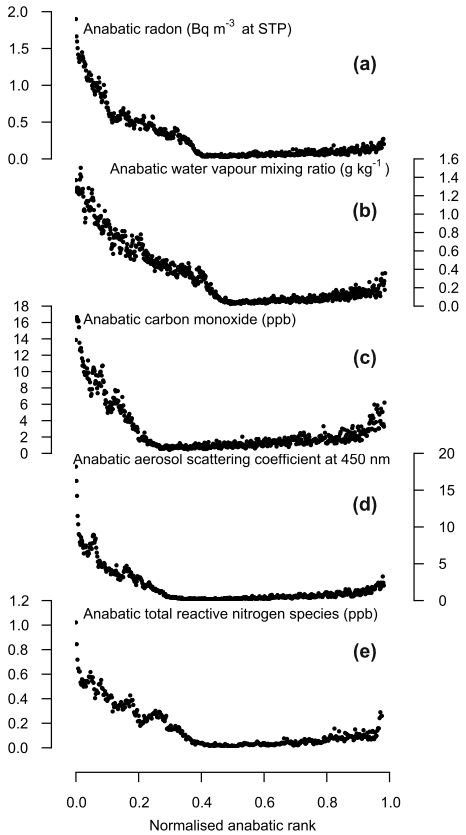

Figure 8. The anabatic contribution, i.e. the daily-mean concentration due to anabatic flows, of several tracers as a function of the anabatic rank normalised by total number of observation days. The minimum in the anabatic concentration marks the boundary between anabatic days, with lower anabatic rank, and non-anabatic days. The increase in anabatic contribution after the minima is an artefact of the method.

ACPD
14, 18083–18126, 2014

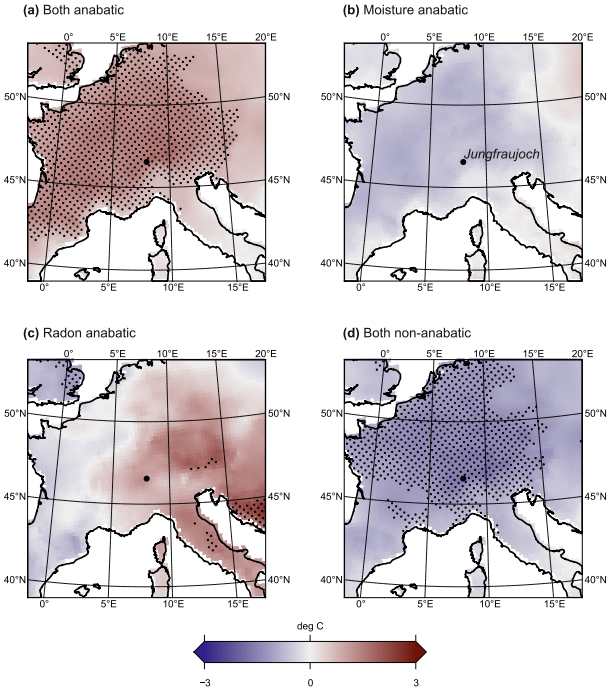

Figure 9. Daily maximum temperature anomalies for months with anabatic flows (April–September, inclusive) defined as the mean of each group minus the mean anomaly for all days with data available. The groups are: **(a)** days which are anabatic according to both radon and *r*, 140 samples; **(b)** anabatic according to *r* but not radon, 68 samples; **(c)** anabatic according to radon but not *r*, 73 samples; and **(d)** non-anabatic according to both tracers, 82 samples. The stippled region indicates a statistically significant difference between the group mean and the full population at the 95 % confidence level according to Welch's *t* test (Press et al., 2007; Welch, 1947). Data are gridded observations from E-OBS (Haylock et al., 2008).

ACPD
14, 18083–18126, 2014

Surface-to-mountaintop transport at the Jungfraujoch

A. D. Griffiths et al.

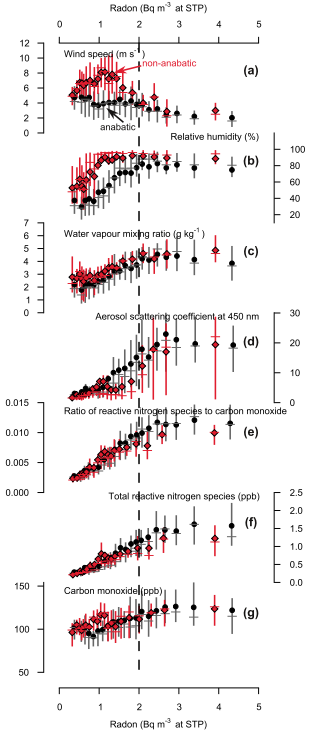

Figure 10. Hourly observations of tracer and meteorological parameters binned according to radon concentration for anabatic and non-anabatic days. The comparison is restricted to: the months when anabatic flows are detected (April–September); hours when the airmass arrives from the north-west; and when the radon and moisture methods agree on the anabatic/non-anabatic classification. For moderate radon concentration, anabatic days are calmer and dryer and aerosols are more abundant. The symbols have the same meaning as Fig. 4.

ACPD
14, 18083–18126, 2014

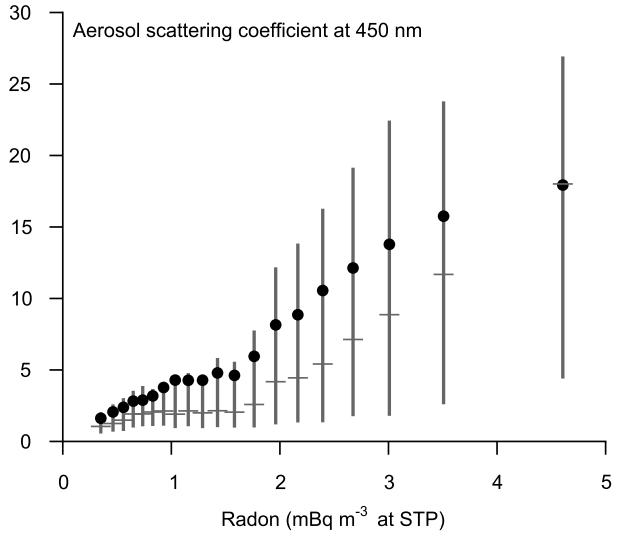

Figure 11. Aerosol scattering coefficient binned by radon concentration. Data are from all months and wind directions. The symbols have the same meaning as Fig. 4.

ACPD
14, 18083–18126, 2014

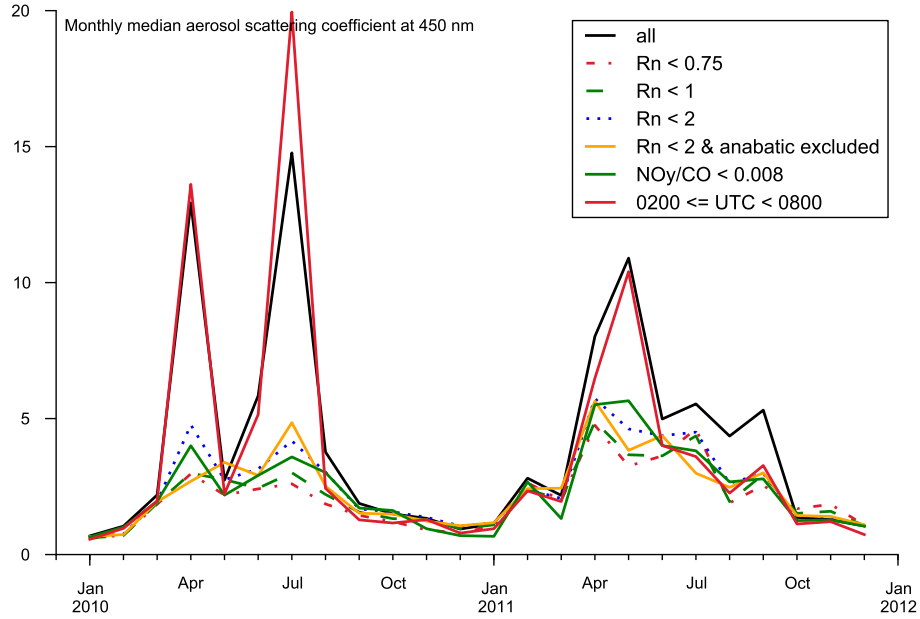

Figure 12. Monthly median aerosol scattering coefficient from different selection criteria: all data; radon concentration less than 0.75, 1, and 2 Bq m^{-3} STP; chemical filter based on NO_y to CO ratio (Pandey Deolal et al., 2013); time-of-day filter. The time-of-day filter is similar to Andrews et al. (2011), keeping data measured during a time window of 03:00–09:00 LT, but we show the median value instead of the mean.

ACPD
14, 18083–18126, 2014

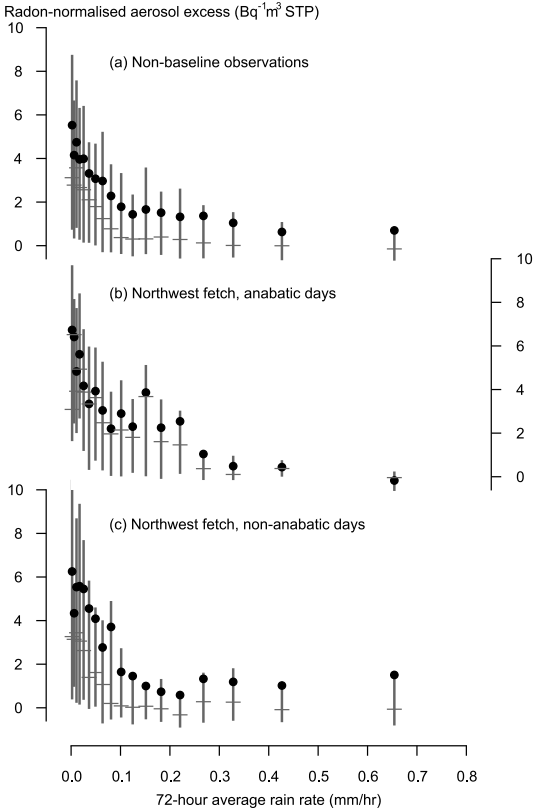

Figure 13. Radon-normalised aerosol excess, a_n, vs. rainfall; a_n is the aerosol scattering coefficient minus baseline divided by the radon concentration minus baseline. Rain rates and trajectories are computed from the 1.0° GFS analysis using Hysplit. Only data from non-baseline conditions are plotted ($> 1\,\mathrm{Bq\,m^{-3}}$ STP) and the panels show **(a)** all non-baseline data, **(b)** north-west fetch/anabatic days, and **(c)** north-west fetch/non-anabatic days. The symbols have the same meaning as Fig. 4.

ACPD
14, 18083–18126, 2014